Emergence of a spin Hall topological Hall effect in the noncollinear phase of the ferrimagnetic insulator terbium-iron garnet

Mehak Loyal [1,*] Akashdeep Akashdeep [1] Edoardo Mangini [1] Edgar Galíndez-Ruales [1] Maja Eich [1] Nan Wang [2] Qianqian Lan [2] Lei Jin [2] Rafal Dunin-Borkowski [2] Timo Kuschel [1] Mathias Kläui [1,3] and Gerhard Jakob [1,†]

[1] *Institute of Physics, Johannes Gutenberg University Mainz, Staudingerweg 7, 55128 Mainz, Germany*

[2] *Ernst Ruska-Centre for Microscopy and Spectroscopy with Electrons (ER-C-1), Forschungszentrum Jülich GmbH, 52425 Jülich, Germany*

[3] *Center for Quantum Spintronics, Department of Physics, Norwegian University of Science and Technology, 7491 Trondheim, Norway*

(Received 13 February 2026; accepted 21 April 2026; published 21 May 2026)

Magnetic compensation in rare-earth iron garnets (REIGs) offers a unique setting in which competing sublattice moments can give rise to non-collinear (canted) magnetic configurations, where the sublattice magnetizations are not aligned with each other or with the external magnetic field. We show that this compensation regime can possibly also host nontrivial magnetic textures. To explore this behavior, we investigated (111)-oriented epitaxial $Tb_3Fe_5O_{12}$/Pt heterostructures across the compensation temperature region using combined transverse magneto-transport and polar Kerr microscopy. Notably, we observe a topological Hall–like signal in the vicinity of the compensation temperature, a feature often interpreted as evidence for skyrmions in the absence of direct imaging. Here, in contrast, complementary Kerr microscopy reveals instead a non-collinear multidomain state which collapses outside the compensation regime, correlating directly with the appearance and disappearance of the spin Hall topological Hall effect (SH-THE) signal. These observations cannot be accounted for by a simple multi-anomalous-Hall-effect model, ruling out common artifacts as the origin, but indicate a topologically nontrivial contribution to the Hall response. These results establish strained REIG films as a tunable platform for exploring topological responses arising from compensation-driven non-collinear ferrimagnetic phases.

DOI: 10.1103/s23p-y6fd

I. INTRODUCTION

The topological Hall effect (THE) is widely regarded as a transport hallmark of topologically nontrivial spin textures that generate an emergent real-space magnetic field [1–5]. Consequently, hump-like anomalies in the Hall response are frequently interpreted as evidence for skyrmion formation [6–9]. Such signatures have been reported across metallic and insulating heterostructures, including rare-earth iron garnets (REIGs) coupled to heavy metals [10–13]. In the case of insulating materials, the THE has been studied with an additional heavy metal layer (e.g., Pt) that provides the ability to utilize the spin Hall magnetoresistance (SMR) [14–17] to investigate the magnetic properties of the insulator via the resistivity change in the heavy metal. For transverse SMR configuration and out-of-plane (OOP) magnetic field orientation, the spin Hall anomalous Hall effect (SH-AHE) can be measured [18]. If the insulating material possesses topologically nontrivial spin textures, the spin Hall topological Hall effect (SH-THE) might be detectable.

In numerous cases, the identification of a topological texture relies entirely on transport, with skyrmion densities inferred from the Hall signal, often without any imaging or independent proof of the underlying spin texture [6]. In systems for which imaging has been performed, the experimentally observed spin structure size frequently contradicts the skyrmion densities required to reproduce the measured Hall signal magnitude, underscoring a mismatch between transport-derived estimates and real-space magnetic configurations [7]. These inconsistencies have led to intense debate over whether the observed anomalies truly reflect real-space topology or arise from more conventional magnetic phenomena. One established alternative is the two-anomalous-Hall-effect (2-AHE) model, in which the Hall response is a superposition of distinct AHE contributions from different magnetic sublattices, interfacial regions, or domain configurations [19–21]. This mechanism can indeed explain several reports of apparent THE-like features and provides a physically meaningful description of systems with multiple magnetic components. As a result, several recent works have emphasized the need for direct complementary magnetic imaging to accompany Hall-based claims of nontrivial spin textures like skyrmions. Without such evidence, attributing Hall anomalies to topological spin textures may be misleading [22].

REIGs constitute a fascinating class of ferrimagnetic insulators whose magnetic properties arise from a three-sublattice structure: two antiferromagnetically coupled iron sublattices on the tetrahedral (d) and octahedral (a) sites, and a rare-earth sublattice on the dodecahedral (c) sites that is antiparallel to the net iron moment. This architecture gives rise to the magnetic compensation temperature T_{comp}, at which the rare-earth and iron sublattice moments cancel exactly, producing zero net magnetization. Below T_{comp}, the rare-earth moments dominate the ferrimagnetic order, whereas above it the iron sublattices prevail; in both regimes, the system remains largely collinear [23]. Near magnetic compensation,

*Contact author: loyalmeh@uni-mainz.de

†Contact author: jakob@uni-mainz.de

in a non-collinear regime, the individual sublattice moments of the garnet are no longer aligned with the net magnetization. The iron moments on the octahedral and tetrahedral sites remain strongly antiferromagnetically coupled and therefore point in opposite directions, while the rare-earth moment has its own orientation set by the competition between weaker RE–Fe exchange fields and crystal-field anisotropy. The net magnetization along the external magnetic field direction is simply the vector sum of these three contributions, and this sum becomes very small near compensation. As a result, even small angular changes of the rare-earth or iron sublattices can produce large relative changes in the net moment, making the system highly sensitive to canting and the formation of non-collinear configurations [24]. Deviations from perfect collinearity have indeed been observed in multiple REIGs, including $(BiYLu)_3(FeGa)_5O_{12}$ [25], and magneto-transport measurements in compensated garnets such as InYGdIG/Pt have directly shown that transport is sensitive to these non-collinear configurations, enabling electrical detection of canted phases [24].

Adding to this complexity is the broader magnetic phase richness found in REIGs, particularly those containing rare-earth ions with strong single-ion anisotropy [26,27]. Terbium iron garnet ($Tb_3Fe_5O_{12}$, TbIG) is a notable example: at low temperatures (below 160 K), it hosts a "double umbrella" configuration, in which the Tb^{3+} magnetic moments form two distinct conical structures with different canting angles [28]. This phase emerges from the competition between the strong uniaxial crystal-field anisotropy of Tb^{3+} and its exchange coupling to the Fe sublattices. While the double-umbrella phase occurs far below T_{comp}, its existence highlights a key point: TbIG is inherently predisposed to non-collinearity, making the high-temperature compensation regime, for which the net magnetization vanishes, a natural setting for complex multidomain and canted textures [28–31].

Here, we have investigated TbIG/Pt heterostructures across the magnetic compensation region using Hall geometry magneto-transport measurements complemented by polar Kerr microscopy. We identify a distinct THE-like contribution that emerges as the SH-THE signature only within a compensation-driven non-collinear multidomain regime. Interestingly, we do not observe skyrmion or bubble-type domains commonly linked to the THE; instead, the domain structure suggests the emergence of a non-collinear magnetic phase, and the magnetic field dependence of the Hall response is inconsistent with a simple 2-AHE. These observations show that the Hall anomaly is tightly correlated with a compensation-driven non-collinear multidomain regime in TbIG. While the present measurements do not directly determine the microscopic vector spin texture, the results are consistent with an emergent-field contribution associated with finite scalar spin chirality in this canted state [32–34], revealing a previously unexplored topological transport regime in ferrimagnetic garnets.

II. METHODS

Epitaxial TbIG thin films with a thickness of ∼9 nm were grown on single-crystal $Gd_3Ga_5O_{12}$ (GGG) (111) substrates by pulsed laser deposition (PLD) in an ultrahigh-vacuum chamber (base pressure $<2 \times 10^{-8}$ mbar). A KrF excimer laser ($\lambda = 248$ nm) with a pulse energy of 130 mJ at 10 Hz was used for ablation. The substrates were heated to 650 °C (ramp rate: 50 K min^{-1}) under 0.2 mbar of oxygen pressure during deposition. After growth, the films were cooled to room temperature at −25 K min^{-1}. Reflection high-energy electron diffraction (RHEED) was used to monitor surface crystallinity *in situ*. A Pt overlayer with a thickness of ∼2 nm was deposited at room temperature by DC magnetron sputtering under an Ar pressure of 0.02 mbar for transverse magneto-transport measurements. To ensure a clean TbIG/Pt interface, the sample was transferred from the PLD chamber to the sputtering system in a vacuum suitcase. Crystallinity and overall growth quality were evaluated by high-resolution X-ray diffraction (HRXRD) performed on a Bruker D8 system. Atomic-scale structural analysis was conducted using a TFS Titan Spectra microscope operated at 300 kV and equipped with a high-brightness field-emission gun, probe Cs corrector, and Super-X EDX detectors [35]. High-angle annular dark-field scanning transmission electron microscopy (HAADF-STEM) images were acquired along the $[11\bar{2}]$ zone axis to characterize the film–substrate interface quality and cation ordering. Fast Fourier transforms (FFTs) of selected regions were used to confirm epitaxial alignment. Structural overlays generated in VESTA aided the identification of cation positions and the comparison with the expected garnet structure [36].

The electrical transport measurements were conducted on the GGG/TbIG/Pt heterostructure using the van der Pauw geometry, employing an RTM2 tensometer. While we measure the transverse resistivity ρ_{xy}, which contains contributions from multiple mechanisms, we refer to it in the following as the Hall response. Magnetic imaging was carried out using a commercially available Evico Magnetics Kerr microscope. The system uses a blue LED illumination source and a charge-coupled-device camera, yielding a field of view of 600 × 400 μm². A perpendicular magnetic field was applied using the Evico OOP electromagnet capable of generating magnetic field strengths of up to ∼900 mT. The sample was mounted directly on a Peltier element for temperature control, calibrated using a Pt100 resistance temperature sensor.

III. RESULTS

A. Growth and structural characteristics

The epitaxial quality of the TbIG films is confirmed by the combined structural probes summarized in Fig. 1. The $\theta/2\theta$ scan [Fig. 1(a)] exhibits a sharp GGG(444) substrate peak together with a TbIG(444) film peak that nearly coincides with it. Although bulk TbIG has a larger lattice parameter (12.44 Å) than GGG (12.36 Å), the near overlap of the peaks indicates that the TbIG thin film deviates from the bulk lattice parameter and is strongly influenced by epitaxial strain. The inset RHEED pattern further confirms the excellent epitaxial quality, revealing streaky features characteristic of a smooth, two-dimensional surface. The HAADF-STEM image acquired from a cross-sectional sample in Fig. 1(b) shows an atomically sharp interface and a well-defined garnet lattice, as highlighted by the corresponding FFT and

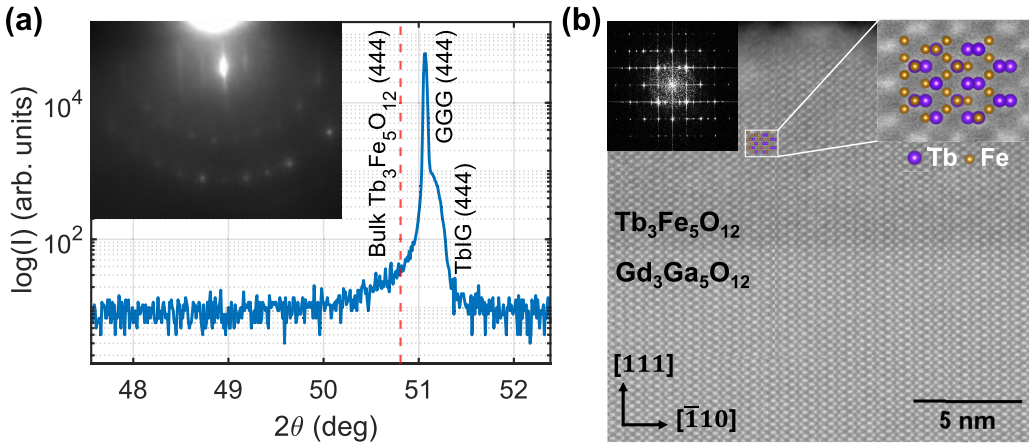

FIG. 1. Structural characterization. (a) $\theta/2\theta$ HRXRD pattern for epitaxial TbIG deposited on GGG(111) substrates. Inset in the figure shows the RHEED pattern after TbIG deposition, highlighting its excellent crystalline properties. (b) HAADF-STEM image across the interface of GGG and TbIG, revealing their atomic-scale structural relationship. The top left inset shows the corresponding FFT of the TbIG layer, and the top right inset shows a magnified region with an overlaid VESTA-generated atomic site map. The purple (Tb) and gold (Fe) markers indicate the projected crystallographic positions of the cations in the TbIG garnet structure, providing a structural reference for the atomic contrast observed in the HAADF-STEM image.

the VESTA-generated structural overlay. Such well-defined structural quality is essential for ferrimagnetic garnets, whose magnetic compensation temperature T_{comp}, the point at which the net magnetization vanishes, can be strongly shifted and sensitively tuned by stoichiometry, strain, and film thickness [37–39]. Although bulk REIGs typically exhibit compensation temperatures well below room temperature, recent studies have shown that T_{comp} can be substantially increased in thin films due to these effects. In the present films, the combined influence of thickness-driven strain results in a compensation temperature near room temperature (≈302 K), a regime particularly favorable for exploring interfacial and ultrafast magnetic phenomena.

B. Compensation-driven evolution of the Hall response

The influence of the compensation point on interfacial magneto-transport is captured in the Hall response, shown in Fig. 2. At temperatures well below and above compensation, for example, at 280 K and 340 K, the Hall loops [Fig. 2(a)] are dominated by the SH-AHE, reflecting the net ferrimagnetic moment of the TbIG layer. The SH-AHE sign change across T_{comp} reveals that it couples to one magnetic sublattice, reversing as the dominant contribution to the total magnetic moment shifts from the rare-earth to the iron sublattice across compensation. This behavior is consistent with the expectation that the Fe sublattice, which dominates the interfacial exchange coupling to Pt, primarily governs the detected Hall response [40]. However, as the system approaches the compensation temperature (≈302 K), the loops develop a pronounced non-monotonic feature along with a sign reversal of the SH-AHE. The raw Hall traces and their ordinary Hall effect (OHE) fits [Fig. 2(b)] enable reliable background subtraction, and the resulting OHE-corrected curves [Fig. 2(c)] clearly resolve two distinct components: a conventional SH-AHE contribution and an additional SH-THE contribution that emerges only in a narrow temperature window around compensation. The extraction procedure is standard: linear high-field fits provide the OHE term, the SH-AHE is defined from the high-field separation of the branches, and the SH-THE component is the deviation from this OHE + SH-AHE baseline. Interestingly, after recombining the extracted SH-AHE and the additional SH-THE contributions, the total signal exhibits an incomplete recovery and retains a characteristic dip [Fig. 2(f)]. This indicates that the magnetic configuration is not fully described by a single collinear component. Even when the Hall loop appears saturated, the reconstructed signal does not return to the expected SH-AHE level, implying that a small degree of canting persists over an extended magnetic field range. This naturally explains that the SH-THE feature is confined to low magnetic fields while the non-collinear background survives to higher magnetic fields, which can be seen in the Kerr images discussed later.

Quantifying the temperature evolution of these components [Fig. 2(f)] shows that the coercivity diverges [Fig. 2(d)], a well-known signature of magnetic compensation in ferrimagnets. The SH-AHE magnitude changes sign upon crossing compensation, consistent with a reversal of the dominant sublattice. The SH-THE contribution appears only within a narrow temperature window (∼298–320 K), peaks sharply near 302 K, and vanishes on either side of T_{comp}.

As a phenomenological estimate, the SH-THE magnitude can be associated with an effective emergent magnetic field using the relation $\rho_{xy}^{\text{THE}} = R_H \cdot B_{\text{eff}}$. Using the experimentally determined values of ρ_{xy}^{THE} (extracted THE resistivity) and R_H (ordinary Hall coefficient), we obtain an effective field scale on the order of ∼0.3−0.9 T, with a maximum near the compensation temperature (see Supplemental Material, Fig. S3). The effective field B_{eff} is often observed to be approximately temperature independent in a system with a skyrmion phase [41–43]. The strong temperature dependence (see Supplemental Material, Sec. IV) indicates that the effect is governed primarily by compensation-driven changes in the underlying magnetic configuration. However, we note that in TbIG/Pt heterostructures, the Hall signal is detected in the Pt layer and depends on interfacial exchange coupling and

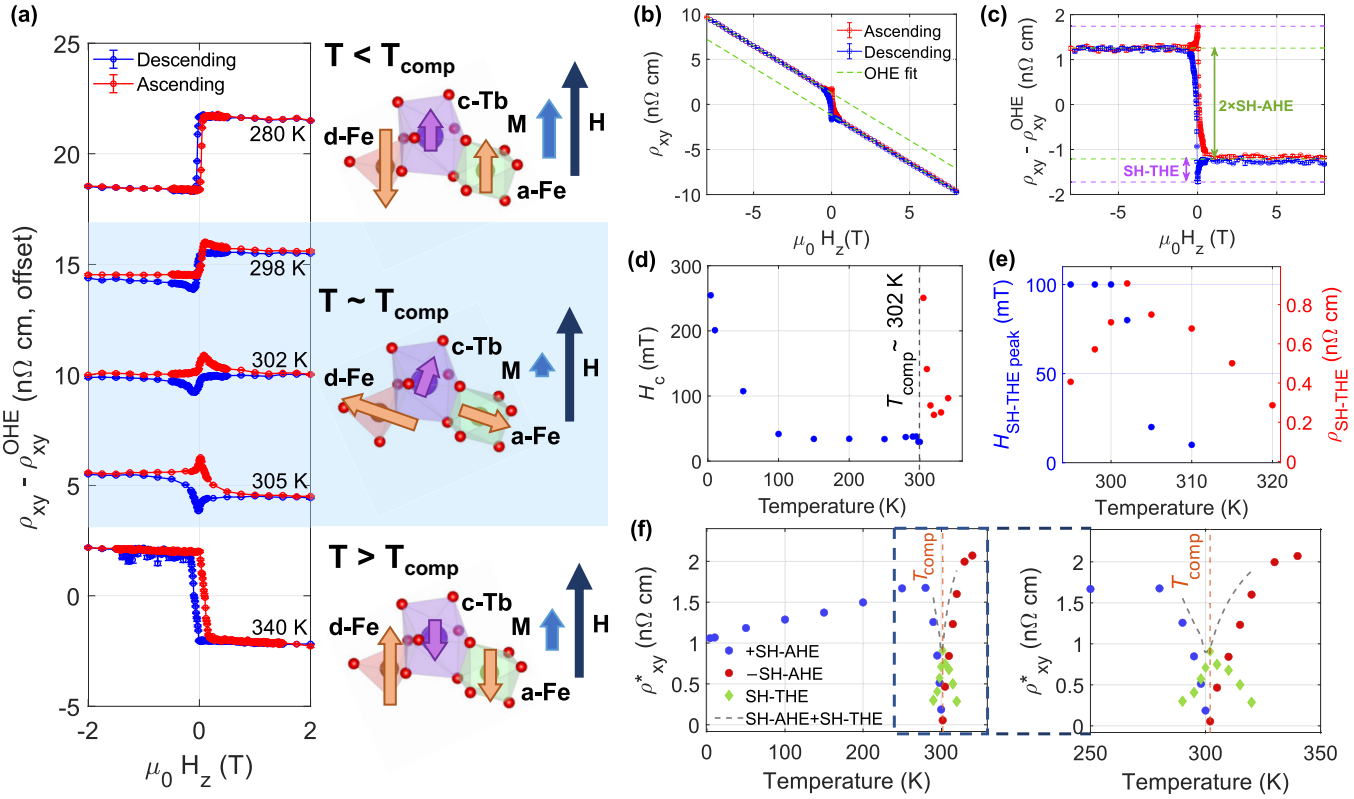

FIG. 2. Temperature-dependent Hall response of GGG/TbIG/Pt heterostructure. (a) Temperature-dependent Hall resistance loops. At 280 K and 340 K, the response is dominated by a single SH-AHE contribution, whereas at temperatures around the compensation point (∼302 K), an additional non-monotonic feature appears together with the SH-AHE sign change across the compensation point. On the right, the corresponding configurations of the magnetic sublattices of TbIG in the non-collinear and collinear phases are shown. (b) Raw Hall data measured at 315 K with linear OHE fits used for background subtraction. (c) OHE-subtracted Hall curves revealing the SH-AHE and the additional SH-THE component at 315 K. (d) Coercivity field H_C as a function of temperature for TbIG with compensation temperature ∼302 K. (e) SH-THE peak amplitude (ρ_{SH-THE}) and corresponding magnetic field position ($H_{SH-THEpeak}$) as a function of temperature. (f) Temperature dependence of the extracted Hall-response components ρ^*_{xy} for the SH-AHE, SH-THE, and their combined signal. SH-THE is finite only near the compensation temperature, while the total SH-AHE+SH-THE curve displays an incomplete recovery, indicating the existence of a non-collinear phase.

spin-charge conversion processes. Accordingly, B_{eff} provides an effective measure of the transverse response induced by the magnetic texture, incorporating both magnetic and interfacial contributions.

A further characteristic feature is the magnetic field position of this additional contribution. The SH-THE peak shifts progressively toward zero magnetic field as the temperature increases above the T_{comp}. It reaches 0 mT between ∼315 K and ∼320 K before disappearing entirely [Fig. 2(e)]. Any 2-AHE model, in contrast, would produce extrema at finite magnetic fields set by the sublattice switching fields. This mismatch rules out the 2-AHE explanation for this system [19–22]. Together, these observations indicate that ultrathin TbIG hosts a compensation-enabled realization of a magnetic state that stabilizes a non-collinear background over a broad magnetic field range, and that within this regime an additional SH-THE contribution emerges.

Similar Hall signal anomalies have been reported previously in TmIG [6,9,10,44,45], but the underlying physics there differs fundamentally from the behavior observed here. In TmIG, the SH-THE signal accompanies a transition from perpendicular to in-plane anisotropy, and its interpretation has involved a range of hypotheses, including interfacial Dzyaloshinskii-Moriya interaction (DMI)–stabilized skyrmions [6] and a 2-AHE model describing the magnetic-proximity effect and spin Hall contributions [45]. Separate studies on TmIG have even reported real-space skyrmions using Kerr microscopy [11,46], whereas in other reports, only a Hall-based SH-THE signature was observed without imaging [6,9,10,44,45], further contributing to the diversity of interpretations. This contrast underscores the inherent ambiguity of transport-only signatures and emphasizes the need to correlate Hall measurements with direct magnetic imaging to determine the origin of SH-THE features.

Given the ambiguity of transport-only signatures, we next employ Kerr microscopy to directly probe the magnetic configuration.

C. Real-space signatures of non-collinearity across compensation

Polar Kerr imaging provides the corresponding real-space picture, summarized in Fig. 3, and offers direct insights into the magnetic domain evolution of TbIG across the

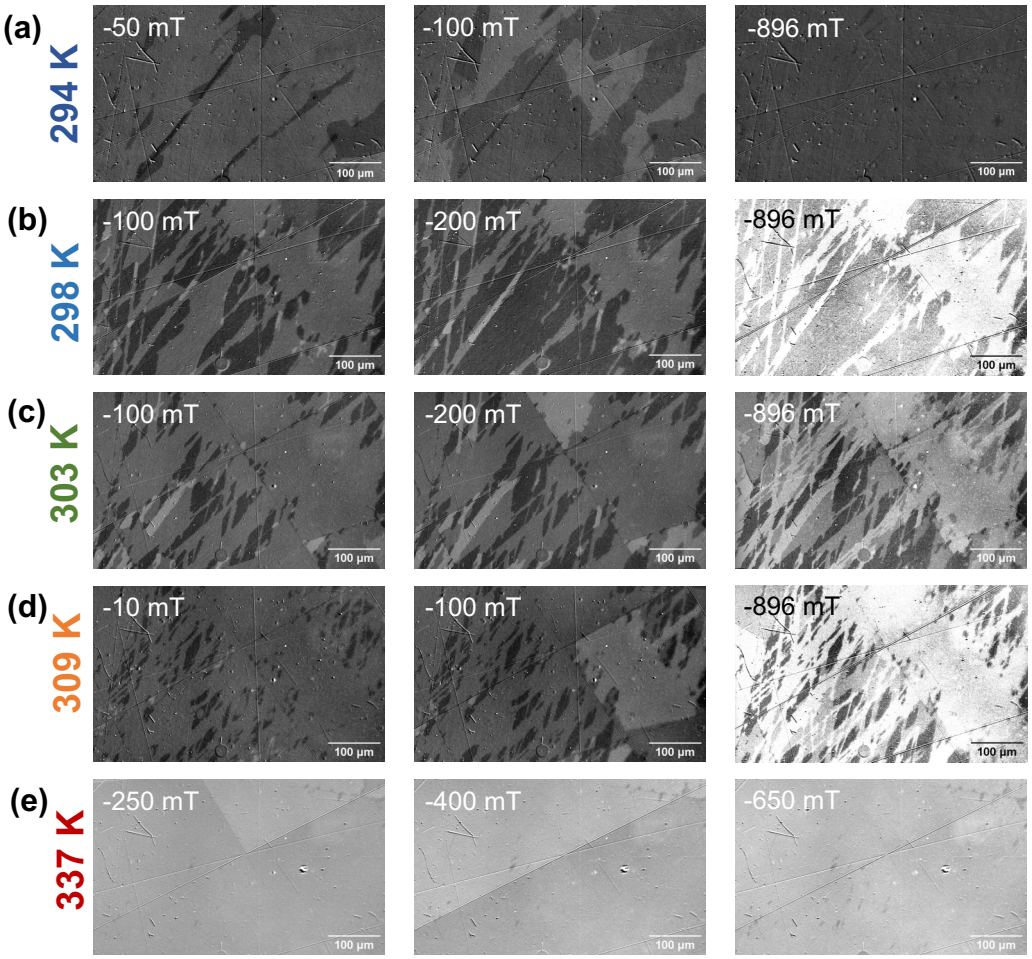

FIG. 3. Polar Kerr imaging across the compensation region. (a)–(e) Difference Kerr images (with respect to the +896 mT state) acquired at selected negative magnetic field strengths for five representative temperatures: 294 K (far below compensation), 298 K (below compensation), 303 K (near compensation), 309 K (above compensation), and 337 K (far above compensation). For 298–309 K, the film cannot be fully saturated with the 896 mT OOP, and the reversal proceeds through mixed multidomain states that correspond to the SH-AHE+SH-THE features seen in transport. Around the compensation temperature (298 K, 303 K, and 309 K), the domain pattern becomes irregular and multidomain, consistent with the non-collinear regime. At 294 K and 337 K, only SH-AHE is observed; the reversal displays predominantly simple collinear domain switching. Magnetic field values: (a) –50, –100, –896 mT; (b) –100, –200, –896 mT; (c) –100, –200, –896 mT; (d) –10, –100, –896 mT; (e) –250, –400, –650 mT.

compensation region, complementing the Hall-transport signatures discussed in Fig. 2. The difference Kerr images recorded at 298 K, 303 K, and 309 K [Figs. 3(a)–3(c)] reveal that the film cannot be fully saturated within the ±896 mT maximum magnetic field available of the OOP coil in the Kerr-microscope. Instead, the magnetic field-driven reversal proceeds through multidomain states. The domains exhibit irregular shapes and multiple contrast levels, indicative of a non-uniform magnetic state. These complex, multidomain patterns appear precisely in the temperature window in which the SH-THE contribution is observed in transport, suggesting a strong link between the real-space magnetic configuration and the observed SH-THE in the compensation regime.

By contrast, at 337 K, well above the compensation point, the magnetic response becomes markedly less complex [Fig. 3(e)]. Here, the film saturates at ∼500 mT, and the reversal proceeds through conventional collinear domain switching with well-separated, uniform domains. In this regime only a single-sign SH-AHE is observed in transport, and no SH-THE features are present. Additionally, images acquired below compensation at 294 K [Fig. 3(a)] show predominantly conventional SH-AHE-dominated contrast with only a very weak indication of an additional contrast level. This indicates that the complex multidomain, non-collinear spin texture is confined to a narrow temperature range around the compensation point. The comparison across temperatures therefore establishes a clear correspondence: the emergence of a multidomain state coincides with the temperature window in which the transport response becomes more complex, including a sign reversal of the SH-AHE and the appearance of an additional SH-THE contribution.

D. Correlated imaging–transport analysis

A more detailed correlation between transport and imaging is presented in Fig. 4, which focuses on the compensation region at 315–317 K. The slight temperature offset between transport (315 K) and imaging (317 K) does not affect these

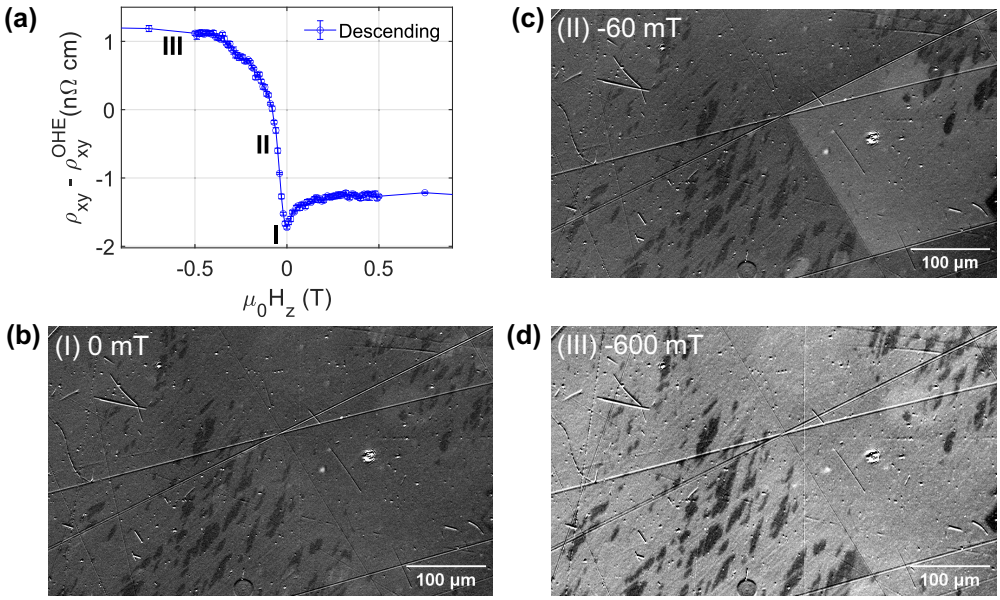

FIG. 4. Correlated Hall transport and Kerr imaging near compensation regime. (a) OHE-subtracted Hall signal measured at 315 K in the descending magnetic field branch, with three characteristic magnetic field positions marked: (I) 0 mT: maximum of the SH-THE contribution; (II) −60 mT: the SH-AHE reversal begins; and (III) −600 mT, the SH-AHE switching is completed. (b)–(d) Polar Kerr difference images recorded at 317 K at the magnetic field strengths indicated in panel (a). The Kerr images are representative of the magnetic configuration within the compensation-region window and do not imply a strict one-to-one correspondence with the transport data at a specific temperature. (b) At (I) 0 mT, a distinct two-level contrast with small, elongated domains appears, coinciding with the SH-THE peak. (c) At (II) −60 mT, large domains nucleate and expand, reflecting the onset of the SH-AHE-driven reversal. (d) At (III) −600 mT, the transport signal reaches the negative-saturation branch, and the Kerr image still shows a multidomain state. This persistence of domains indicates that the film retains a canted, non-collinear ferrimagnetic state to magnetic field values well above the narrow window in which the SH-THE feature arises.

conclusions; in both cases, the SH-THE feature peaks at 0 mT within the same compensation-driven non-collinear regime. The transport and Kerr measurements were performed in two independent setups with separately calibrated temperature readout. In the transport measurements, performed in a cryostat, the sample temperature is measured at the end of the probe rod rather than directly at the sample position, which can also lead to an additional offset between the recorded and actual sample temperature. In the Kerr measurements, temperature was regulated using a Peltier element, which can introduce small offsets in the absolute temperature compared to the transport setup. We note that the Kerr images shown are representative of the magnetic state within this regime and are not intended to correspond to an exact one-to-one mapping with the transport measurement at a specific temperature. Therefore, the comparison is not based on exact sub-kelvin matching of the absolute temperature values, but on reproducible measurements within the same narrow compensation-region window for which both the SH-THE-like anomaly and the complex multidomain Kerr contrast are observed. In particular, the relevant Kerr measurements were chosen within the temperature interval for which the transport anomaly remains centered near zero magnetic field, and the corresponding Hall signal saturates well within the available magnetic field range (∼896 mT).

The Hall signal at 315 K [Fig. 4(a)], taken on the descending branch, highlights three representative magnetic field values: (I) 0 mT: the SH-THE peak is most pronounced; (II) −60 mT: the SH-AHE switching region; and (III) −600 mT: the negative SH-AHE-saturation branch.

The Kerr images recorded at the corresponding magnetic field values [Figs. 4(b)–4(d)] reveal how each transport feature maps onto a distinct magnetic configuration. At (I) 0 mT [Fig. 4(b)], when the SH-THE response peaks, the film exhibits a two-level, fragmented contrast composed of small, elongated domains, consistent with the non-collinear texture associated with the SH-THE response in ρ_{xy}. At (II) −60 mT [Fig. 4(c)], which lies within the SH-AHE reversal window, large reversed domains begin to nucleate and expand even though the earliest switching step occurs well after the topological Hall peak vanishes. At (III) −600 mT [Fig. 4(d)], the Hall signal has reached the negative-saturation branch. Yet, the Kerr images still display residual black and white multidomain contrast at magnetic field values for which the SH-AHE signal appears saturated. While the Kerr measurement itself does not directly probe canting angles, the persistence of opposite-contrast domains at magnetic fields in which the SH-AHE signal has reached apparent saturation implies that the magnetization cannot be fully collinear. In a truly saturated (collinear) state, the Kerr contrast would be uniform as in Fig. 3(d); therefore, the observed multidomain pattern is consistent with a canted magnetic configuration.

A key question is whether the Hall anomaly at 315 K could arise from a trivial superposition of two anomalous Hall contributions (2-AHE), originating from two domain populations with different coercivities. While the transport data already disfavors this interpretation, based on the evolution of the SH-THE peak position with temperature. In the following, Kerr imaging provides an independent verification of this interpretation. In a 2-AHE scenario, the additional "hump"

in ρ_{xy} should persist until the higher-coercivity population completes its switching. Instead, we find that the SH-THE signal collapses well before the second population reverses, which is incompatible with a simple 2-AHE superposition. The persistence of a multidomain structure well past the SH-THE peak underscores the non-collinear nature of the TbIG layer near compensation: the non-collinear magnetic structure remains stable even under high magnetic fields, consistent with transport showing no additional switching up to 8 T [Fig. 2(b)].

IV. DISCUSSION

The observation of an additional Hall contribution in TbIG/Pt near the compensation temperature raises the question of its microscopic origin. While the experimental results place strong constraints on possible mechanisms, ruling out a simple superposition of anomalous Hall contributions alone does not uniquely establish a THE. In the following, we therefore distinguish between mechanisms that can be excluded, those that remain possible but appear less consistent with the data, and the interpretation that is most compatible with the combined transport and imaging results.

To clarify the origin of the SH-THE signal, we performed additional measurements on thicker TbIG films (see Supplemental Material, Sec. I). In a 20 nm film, the temperature window supporting the SH-THE response collapses to a narrow ± 1 K interval around the compensation point, accompanied by a reduced signal amplitude. This strong thickness dependence indicates that the effect is confined to the ultrathin regime and suggests a significant role of strain and interfacial contributions. While such behavior could in principle be associated with interfacial DMI, it is important to note that the magnitude of DMI in garnet systems is generally weak on the order of a few $\mu J\,m^{-2}$ compared to exchange and anisotropy energies [47,48]. The Kerr microscopy reveals extended multidomain structures rather than localized topological objects, indicating that the magnetic state is governed primarily by compensation-driven canting and domain-wall physics. This interpretation is further supported by device-level measurements: in a patterned 10 μm wide Hall bar, the SH-THE anomaly persists, but its magnetic field profile evolves from a sharp peak into a plateau-like feature. Such behavior is consistent with enhanced domain-wall pinning at device edges, which modifies the reversal dynamics without altering the underlying compensation-driven mechanism (see Supplemental Material, Secs. II and III). Consequently, the system may not be able to stabilize isolated skyrmionic textures, which require DMI strengths approaching a critical threshold set by the competition between exchange and anisotropy.

Excluding a simple superposition of 2-AHE channels does not by itself uniquely establish a topological Hall mechanism. In TbIG/Pt heterostructures, additional contributions may in principle arise from interfacial electronic reconstruction in Pt, proximity-induced AHE, or magnetic field-dependent chiral domain textures. In the present case, however, several observations constrain these possibilities. First, the SH-THE feature appears only within a narrow temperature window around the compensation point and vanishes outside this regime, whereas a proximity-induced anomalous Hall contribution in Pt is expected to scale with the interfacial magnetization and therefore evolve more smoothly with temperature, typically increasing upon cooling. Second, the peak position shifts continuously toward zero magnetic field and later collapses at zero magnetic field, which is inconsistent with independent magnetic contributions or spatial phase separation that would produce features tied to finite switching fields. Third, Kerr microscopy reveals the emergence of a non-collinear multidomain state only within the same temperature window in which the SH-THE signal is observed, directly linking the transport anomaly to a distinct magnetic configuration. Magneto-optical measurements support the presence of a canted, non-collinear magnetic state in this regime. While non-collinearity alone does not guarantee a finite scalar spin chirality, the coincidence of the Hall anomaly with a non-collinear magnetic texture places strong constraints on possible mechanisms. In particular, although chiral spin textures such as skyrmions or bubble-like domains below the resolution limit of Kerr microscopy cannot be completely excluded, the data do not require the presence of a well-defined topological texture. Instead, a finite scalar spin chirality arising from a spatially varying, non-coplanar spin configuration provides the most self-consistent explanation of the observed behavior. The close correspondence between the Hall anomaly and the regime of non-collinear magnetic order therefore supports an interpretation in terms of an emergent-field contribution associated with non-coplanar spin structure.

The scalar spin chirality is defined as $\chi_{ijk} = \boldsymbol{S}_i \cdot (\boldsymbol{S}_j \times \boldsymbol{S}_k)$, which represents the solid angle subtended by three neighboring spins. A finite value of χ_{ijk} requires a non-coplanar spin configuration, whereas collinear or coplanar arrangements yield zero scalar chirality. We note that TbIG is known to host non-collinear magnetic configurations, such as the double umbrella phase reported at low temperatures in bulk crystals [28–31]. In this phase, the Tb sublattice adopts a non-coplanar arrangement. In contrast, our measurements probe the vicinity of the magnetic compensation point in thin films. Therefore, we view the existence of the double umbrella structure as an indication that non-coplanar spin configurations are energetically accessible in this material. In thin films, symmetry breaking arising from interface/strain may partially lift net scalar spin chirality cancellation and potentially enable a finite emergent field. Within this framework, finite scalar spin chirality can originate from spatially varying, non-coplanar configurations across domains and sublattices, with DMI, acting only as a secondary symmetry-breaking perturbation to prevent complete cancellation upon spatial averaging.

The Supplemental Material includes measurements on thicker films and patterned Hall-bar devices, as well as the temperature dependence of the extracted effective field B_{eff} [49]. While the magnitude and magnetic field profile of the SH-THE response vary, the overall phenomenology remains consistent across all samples, underscoring the robustness of the observed behavior.

V. CONCLUSION

In summary, we demonstrate that $Tb_3Fe_5O_{12}$ thin films host a compensation-enabled non-collinear magnetic state that can stabilize nontrivial spin textures associated with the

SH-THE signal. By combining transverse magneto-transport with magnetic field-resolved polar Kerr microscopy, we directly correlate the emergence of this transport anomaly with the appearance of a non-collinear multidomain configuration that exists only within a narrow temperature interval around magnetic compensation. Outside this regime, the domain structure reverts to conventional collinear reversal, and the Hall anomaly vanishes. The observed Hall behavior cannot be accounted for by a simple superposition of anomalous Hall components and instead is most consistently interpreted as an emergent-field-like Hall contribution associated with the compensation-enabled non-collinear canted state, although direct proof of scalar spin chirality will require further microscopic or sublattice-resolved probes.

ACKNOWLEDGMENTS

M.L., A.A., E.M., E.G.-R., M.E., T.K., M.K., and G.J. gratefully acknowledge the funding support from the Deutsche Forschungsgemeinschaft (DFG) under the framework of the Collaborative Research Center TRR 173–268565370 Spin+X (Project B02, A01, and A12), TRR 288–422213477 Elasto-Q-Mat (Project A12). This project has also received funding from the European Research Council (ERC) under the Marie Skłodowska-Curie Grant Agreement No. 101119608 ("TOPOCOM") and under the European Union's Horizon 2020 research and innovation programme Grant No. 856538 ("3D MAGiC"). This work contains results obtained from the experiments performed at the Ernst Ruska-Centre (ER-C) for Microscopy and Spectroscopy with electrons at the Forschungszentrum Jülich (FZJ) in Germany. The ER-C beam-time access was provided via the DFG Core Facility Project [External ER-C E-047]. M.K. acknowledges support by the Research Council of Norway through its Centers of Excellence funding scheme under Project No. 262633 "QuSpin."

DATA AVAILABILITY

The data that support the findings of this article are openly available [50].

[1] H. Wang, Y. Dai, G. M. Chow, and J. Chen, Topological Hall transport: Materials, mechanisms and potential applications, Prog. Mater Sci. **130**, 100971 (2022).

[2] Y. He, S. Schneider, T. Helm, J. Gayles, D. Wolf, I. Soldatov, H. Borrmann, W. Schnelle, R. Schaefer, G. H. Fecher, B. Rellinghaus, and C. Felser, Topological Hall effect arising from the mesoscopic and microscopic non-coplanar magnetic structure in MnBi, Acta Mater. **226**, 117619 (2022).

[3] X. Lv, Y. Huang, K. Pei, C. Yang, T. Zhang, W. Li, G. Cao, J. Zhang, Y. Lai, and R. Che, Manipulating the magnetic bubbles and topological Hall effect in 2D magnet Fe_5GeTe_2, Adv. Funct. Mater. **34**, 2308560 (2023).

[4] A. Thomas, D. Pohl, A. Tahn, H. Schlörb, S. Schneider, D. Kriegner, S. Beckert, P. Vir, M. Winter, C. Felser, and B. Rellinghaus, In-situ monitoring the magnetotransport signature of topological transitions in a chiral magnet, Small Methods **9**, 2401875 (2025).

[5] M. V. Sapozhnikov, N. S. Gusev, S. A. Gusev, D. A. Tatarskiy, Y. V. Petrov, A. G. Temiryazev, and A. A. Fraerman, Direct observation of topological Hall effect in Co/Pt nanostructured films, Phys. Rev. B **103**, 054429 (2021).

[6] Q. Shao, Y. Liu, G. Yu, S. K. Kim, X. Che, C. Tang, Q. L. He, Y. Tserkovnyak, J. Shi, and K. L. Wang, Topological Hall effect at above room temperature in heterostructures composed of a magnetic insulator and a heavy metal, Nat. Electron. **2**, 182 (2019).

[7] L. Vistoli, W. Wang, A. Sander, Q. Zhu, B. Casals, R. Cichelero, A. Barthélémy, S. Fusil, G. Herranz, S. Valencia, R. Abrudan, E. Weschke, K. Nakazawa, H. Kohno, J. Santamaria, W. Wu, V. Gracia, and M. Bibes, Giant topological Hall effect in correlated oxide thin films, Nat. Phys. **15**, 67 (2019).

[8] S. Sugimoto, Y. K. Takahashi, and S. Kasai, Near-room temperature topological Hall effect at spin reorientations in sputtered $NdCo_{5-x}Cu_x$ thin film, Appl. Phys. Lett. **121**, 182404 (2022).

[9] P. Li, J. Ding, S. S. L. Zhang, J. Kally, T. Pillsbury, O. G. Heinonen, G. Rimal, C. Bi, A. DeMann, S. B. Field, W. Wang, J. Tang, J. S. Jiang, A. Hoffmann, N. Samarth, and M. Wu, Topological Hall effect in a topological insulator interfaced with a magnetic insulator, Nano Lett. **21**, 84 (2020).

[10] T. N. Nunley, S. Guo, L. J. Chang, D. Lujan, J. Choe, S. F. Lee, F. Yang, and X. Li, Quantifying spin Hall topological Hall effect in ultrathin $Tm_3Fe_5O_{12}$/Pt bilayers, Phys. Rev. B **106**, 014415 (2022).

[11] S. Ding, A. Ross, R. Lebrun, S. Becker, K. Lee, I. Boventer, S. Das, Y. Kurokawa, S. Gupta, J. Yang, G. Jakob, and M. Kläui, Interfacial Dzyaloshinskii-Moriya interaction and chiral magnetic textures in a ferrimagnetic insulator, Phys. Rev. B **100**, 100406(R) (2019).

[12] W. Zhang, B. Balasubramanian, A. Ullah, R. Pahari, X. Li, L. Yue, S. R. Valloppilly, A. Sokolov, R. Skomski, and D. J. Sellmyer, Comparative study of topological Hall effect and skyrmions in NiMnIn and NiMnGa, Appl. Phys. Lett. **115**, 172404 (2019).

[13] W. Zhang, B. Balasubramanian, Y. Sun, A. Ullah, R. Skomski, R. Pahari, S. R. Valloppilly, X. Z. Li, C. Z. Wang, K. M. Ho, and D. J. Sellmyer, Magnetism and topological Hall effect in antiferromagnetic Ru_2MnSn-based Heusler compounds, J. Magn. Magn. Mater. **537**, 168104 (2021).

[14] H. Nakayama, M. Althammer, Y. T. Chen, K. Uchida, Y. Kajiwara, D. Kikuchi, T. Ohtani, S. Geprägs, M. Opel, S. Takahashi, R. Gross, G. E. W. Bauer, S. T. B. Goennenwein, and E. Saitoh, Spin Hall magnetoresistance induced by a nonequilibrium proximity effect, Phys. Rev. Lett. **110**, 206601 (2013).

[15] M. Althammer, S. Meyer, H. Nakayama, M. Schreier, S. Altmannshofer, M. Weiler, H. Huebl, S. Geprägs, M. Opel, R. Gross, D. Meier, C. Klewe, T. Kuschel, J. M. Schmalhorst, G. Reiss, L. Shen, A. Gupta, Y. T. Chen, G. E. W. Bauer, E. Saitoh, and S. T. B. Goennenwein, Quantitative study of the

spin Hall magnetoresistance in ferromagnetic insulator/normal metal hybrids, Phys. Rev. B **87**, 224401 (2013).

[16] Y. T. Chen, S. Takahashi, H. Nakayama, M. Althammer, S. T. B. Goennenwein, E. Saitoh, and G. E. W. Bauer, Theory of spin Hall magnetoresistance, Phys. Rev. B **87**, 144411 (2013).

[17] N. Vlietstra, J. Shan, V. Castel, B. J. van Wees, and J. Ben Youssef, Spin-Hall magnetoresistance in platinum on yttrium iron garnet: Dependence on platinum thickness and in-plane/out-of-plane magnetization, Phys. Rev. B **87**, 184421 (2013).

[18] S. Meyer, R. Schlitz, S. Geprägs, M. Opel, H. Huebl, R. Gross, and S. T. B. Goennenwein, Anomalous Hall effect in YIG|Pt bilayers, Appl. Phys. Lett. **106**, 132402 (2015).

[19] D. Kan, T. Moriyama, K. Kobayashi, and Y. Shimakawa, Alternative to the topological interpretation of the transverse resistivity anomalies in $SrRuO_3$, Phys. Rev. B **98**, 180408(R) (2018).

[20] L. Tai, B. Dai, J. Li, H. Huang, S. K. Chong, K. L. Wong, H. Zhang, P. Zhang, P. Deng, C. Eckberg, G. Qiu, H. He, D. Wu, S. Xu, A. Davydov, R. Wu, and K. L. Wang, Distinguishing the two-component anomalous Hall effect from the topological Hall effect, ACS nano **16**, 17336 (2022).

[21] T. Fu, S. Li, X. Feng, Y. Cui, J. Yao, B. Wang, J. Cao, Z. Shi, D. Xue, and X. Fan, Complex anomalous Hall effect of CoGd alloy near the magnetization compensation temperature, Phys. Rev. B **103**, 064432 (2021).

[22] G. Kimbell, C. Kim, W. Wu, M. Cuoco, and J. W. A. Robinson, Challenges in identifying chiral spin textures via the topological Hall effect, Commun. Mater. **3**, 19 (2022).

[23] Y. Yang, T. Liu, L. Bi, and L. Deng, Recent advances in development of magnetic garnet thin films for applications in spintronics and photonics, J. Alloys Compd. **860**, 158235 (2021).

[24] K. Ganzhorn, J. Barker, R. Schlitz, B. A. Piot, K. Ollefs, F. Guillou, F. Wilhelm, A. Rogalev, M. Opel, M. Althammer, S. Geprägs, H. Huebl, R. Gross, G. E. W. Bauer, and S. T. B. Goennenwein, Spin Hall magnetoresistance in a canted ferrimagnet, Phys. Rev. B **94**, 094401 (2016).

[25] D. A. Suslov, P. M. Vetoshko, A. V. Mashirov, S. V. Taskaev, S. N. Polulyakh, V. N. Berzhansky, and V. G. Shavrov, Non-collinear phase in rare-earth iron garnet films near the compensation temperature, Crystals **13**, 1297 (2023).

[26] Y. Li, Y. Duan, M. Wang, L. Lang, Y. Zhang, K. Shen, Z. Shi, and S. M. Zhou, Abnormal spin Seebeck effect near compensation temperature in $Tb_3Fe_5O_{12}$ garnet films, npj Spintronics **3**, 15 (2025).

[27] Y. Li, Y. Duan, M. Wang, L. Lang, Y. Zhang, M. Yang, J. Li, W. Fan, K. Shen, Z. Shi, and S. M. Zhou, Giant magnon-polaron anomalies in spin seebeck effect in double umbrella-structured $Tb_3Fe_5O_{12}$ films, Phys. Rev. Lett. **132**, 056702 (2024).

[28] M. Lahoubi and B. Ouladdiaf, Anomalous magnetic reordering in magnetodielectric terbium iron garnet at low temperatures, J. Magn. Magn. Mater. **373**, 108 (2015).

[29] M. Lahoubi, M. Guillot, A. Marchand, F. Tcheou, and E. Roudault, Double umbrella structure in terbium iron garnet, IEEE Trans. Magn. **20**, 1518 (1984).

[30] B. Tomasello, D. Mannix, S. Geprägs, and T. Ziman, Origin and dynamics of umbrella states in rare-earth iron garnets, Ann. Phys. **447**, 169117 (2022).

[31] M. Lahoubi, Magnetic study of the low temperature anomalies in the magnetodielectric terbium iron garnet, Physica B **536**, 96 (2018).

[32] N. Mohanta, S. Okamoto, and E. Dagotto, Planar topological Hall effect from conical spin spirals, Phys. Rev. B **102**, 064430 (2020).

[33] G. Go, D. P. Goli, N. Esaki, Y. Tserkovnyak, and S. K. Kim, Scalar spin chirality Hall effect, arXiv:2411.03679.

[34] A. Rajan, T. G. Saunderson, F. R. Lux, R. Y. Díaz, H. M. Abdullah, A. Bose, B. Bednarz, J. Y. Kim, D. Go, T. Hajiri, G. Shukla, O. Gomonay, Y. Yao, W. Feng, H. Asano, U. Schwingenschlögl, L. López-Díaz, J. Sinova, G. Jakob, Y. Mokrousov, A. Manchon, and M. Kläui, Higher-order Hall response arises from octupole order and scalar spin chirality in a noncollinear antiferromagnet, Commun. Mater. **7**, 73 (2026).

[35] A. Kovács, R. Schierholz, and K. Tillmann, FEI Titan G2 80–200 CREWLEY, J. Large-Scale Research Facilities **2**, A43 (2016).

[36] K. Momma and F. Izumi, VESTA: A three-dimensional visualization system for electronic and structural analysis, J. Appl. Crystallogr. **41**, 653 (2008).

[37] Z. Xu, Q. Liu, Y. Ji, X. Li, J. Li, J. Wang, and L. Chen, Strain-tunable interfacial Dzyaloshinskii–Moriya interaction and spin-Hall topological Hall effect in $Pt/Tm_3Fe_5O_{12}$ heterostructures, ACS Appl. Mater. Interfaces **14**, 16791 (2022).

[38] J. M. Liang, X. W. Zhao, Y. K. Liu, P. G. Li, S. M. Ng, H. F. Wong, W. F. Cheng, Y. Zhou, J. Y. Dai, C. L. Mak, and C. W. Leung, The thickness effect on the compensation temperature of rare-earth garnet thin films, Appl. Phys. Lett. **122**, 242401 (2023).

[39] E. Rosenberg, J. Bauer, E. Cho, A. Kumar, J. Pelliciari, C. A. Occhialini, S. Ning, A. Kaczmarek, R. Rosenberg, J. W. Freeland, Y. C. Chen, J. P. Wang, J. LeBeau, R. Comin, F. M. F. de Groot, and C. A. Ross, Revealing site occupancy in a complex oxide: Terbium iron garnet, Small **19**, 2300824 (2023).

[40] Q. Shao, A. Grutter, Y. Liu, G. Yu, C. Y. Yang, D. A. Gilbert, E. Arenholz, P. Shafer, X. Che, C. Tang, M. Aldosary, A. Navabi, Q. L. He, B. J. Kirby, J. Shi, and K. L. Wang, Exploring interfacial exchange coupling and sublattice effect in heavy metal/ferrimagnetic insulator heterostructures using Hall measurements, x-ray magnetic circular dichroism, and neutron reflectometry, Phys. Rev. B **99**, 104401 (2019).

[41] Y. Li, L. Zhang, Q. Zhang, C. Li, T. Yang, Y. Deng, L. Gu, and D. Wu, Emergent topological Hall effect in $La_{0.7}Sr_{0.3}MnO_3/SrIrO_3$ heterostructures, ACS Appl. Mater. Interfaces **11**, 21268 (2019).

[42] N. Kanazawa, Y. Onose, T. Arima, D. Okuyama, K. Ohoyama, S. Wakimoto, K. Kakurai, S. Ishiwata, and Y. Tokura, Large topological Hall effect in a short-period helimagnet MnGe, Phys. Rev. Lett. **106**, 156603 (2011).

[43] T. Tanigaki, K. Shibata, N. Kanazawa, X. Yu, Y. Onose, H. S. Park, D. Shindo, and Y. Tokura, Real-space observation of short-period cubic lattice of skyrmions in MnGe, Nano Lett. **15**, 5438 (2015).

[44] A. J. Lee, S. Guo, J. Flores, B. Wang, N. Bagués, D. W. McComb, and F. Yang, Investigation of the role

of rare-earth elements in spin-Hall topological Hall effect in Pt/ferrimagnetic-garnet bilayers, Nano Lett. **20**, 4667 (2020).

[45] S. Ding, Z. Liang, C. Yun, R. Wu, M. Xue, Z. Lin, A. Ross, S. Becker, W. Yang, X. Ma, D. Chen, K. Sun, G. Jakob, M. Kläui, and J. Yang, Anomalous Hall effect in magnetic insulator heterostructures: Contributions from spin-Hall and magnetic-proximity effects, Phys. Rev. B **104**, 224410 (2021).

[46] S. Vélez, S. Ruiz-Gómez, J. Schaab, E. Gradauskaite, M. S. Wörnle, P. Welter, B. J. Jacot, C. L. Degen, M. Trassin, M. Fiebig, and P. Gambardella, Current-driven dynamics and ratchet effect of skyrmion bubbles in a ferrimagnetic insulator, Nat. Nanotechnol. **17**, 834 (2022).

[47] L. Caretta, E. Rosenberg, F. Büttner, T. Fakhrul, P. Gargiani, M. Valvidares, Z. Chen, P. Reddy, D. A. Muller, C. A. Ross, and G. S. D. Beach, Interfacial Dzyaloshinskii-Moriya interaction arising from rare-earth orbital magnetism in insulating magnetic oxides, Nat. Commun. **11**, 1090 (2020).

[48] S. Fedel, M. Villa, S. Damerio, E. Demiroglu, C. Deger, J. Gazquez, and C. O. Avci, Evidence of long-range Dzyaloshinskii–Moriya interaction at ferrimagnetic insulator/nonmagnetic metal interfaces, Adv. Funct. Mater. **35**, 2418653 (2025).

[49] See Supplemental Material at http://link.aps.org/supplemental/10.1103/s23p-y6fd for measurements on thicker films and Hall-bar devices and temperature dependence of B_{eff}.

[50] M. Loyal, A. Akashdeep, E. Mangini, E. Galíndez-Ruales, M. Eich, N. Wang, Q. Lan, L. Jin, R. Dunin-Borkowski, T. Kuschel, M. Kläui, and G. Jakob, Emergence of a spin Hall topological Hall effect in the non-collinear phase of the ferrimagnetic insulator terbium-iron garnet [Data set], Zenodo (2026), https://doi.org/10.5281/zenodo.18836464.